NASA Contractor Report 187461

ICASE Report 90-78

ICASE

THE ROUTE TO CHAOS FOR THE KURAMOTO-SIVASHINSKY EQUATION

Demetrios T. Papageorgiou
Yiorgos S. Smyrlis

NASA

National Aeronautics and
Space Administration

Langley Research Center
Hampton, Virginia 23665-5225

The route to chaos for the Kuramoto–Sivashinsky equation.[1]

Demetrios T. Papageorgiou
Department of Mathematics and
Center for Applied Mathematics and Statistics
New Jersey Institute of Technology
Newark, New Jersey 07102

Yiorgos S. Smyrlis
Department of Mathematics
University of California at Los Angeles
Los Angeles, California 90024-1555

ABSTRACT

We present the results of extensive numerical experiments of the spatially periodic initial value problem for the Kuramoto-Sivashinsky equation. Our concern is with the asymptotic nonlinear dynamics as the dissipation parameter decreases and spatio-temporal chaos sets in. To this end the initial condition is taken to be the same for all numerical experiments (a single sine wave is used) and the large time evolution of the system is followed numerically. Numerous computations were performed to establish the existence of windows, in parameter space, in which the solution has the following characteristics as the viscosity is decreased: A steady fully modal attractor to a steady bimodal attractor to another steady fully modal attractor to a steady trimodal attractor to a periodic (in time) attractor, to another steady fully modal attractor, to another time-periodic attractor, to a steady tetramodal attractor, to another time-periodic attractor having a full sequence of period-doublings (in the parameter space) to chaos. Numerous solutions are presented which provide conclusive evidence of the period-doubling cascades which precede chaos for this infinite-dimensional dynamical system. These results permit a computation of the lengths of subwindows which in turn provide an estimate for their successive ratios as the cascade develops. A calculation based on the numerical results is also presented to show that the period doubling sequences found here for the Kuramoto-Sivashinsky equation, are in complete agreement with Feigenbaum's universal constant of 4.669201609... . Some preliminary work shows several other windows following the first chaotic one including periodic, chaotic and a steady octamodal window; however the windows shrink significantly in size to enable concrete quantitative conclusions to be made.

1. Introduction.

The present study is concerned with the long time behavior of the one-dimensional Kuramoto-Sivashinsky (KS) equation, conveniently normalized as

$$u_t + uu_x + u_{xx} + \nu u_{xxxx} = 0 \quad ,$$

$$(x,t) \in \mathbf{R}^1 \times \mathbf{R}^+ \quad , \tag{1.1}$$

$$u(x,0) = u_0(x) \quad , \quad u(x+2\pi,t) = u(x,t) \quad .$$

The parameter ν is positive and takes the role of the *viscosity* of the system.

The long time behavior of the KS equation is characterized by the negative - therefore destabilizing - second order diffusion, the positive - therefore stabilizing - fourth order dissipation and the non-linear coupling term. As soon as the value of ν decreases below 1 at least one Fourier frequency becomes unstable in the linearized model. Nevertheless the solution does not grow exponentially fast as the linear analysis around the null state would suggest but instead stays bounded due to the transfer of energy from the linearly unstable low modes, the number of which is $\text{mod}(\nu^{-1/2})$, to the linearly stable high modes. The previous statement has been observed numerically and also established analytically (see Constantin et al. [8].)

A very attractive feature of (1.1), is that even though it appears to be a very simple partial differential equation it produces complicated dynamics in both space and time (chaotic behavior). The equation arises in a variety of physical problems, such as in chemical physics for propagation of concentration waves (Kuramoto [24], Kuramoto and Tsuzuki [25],[26]), plasma physics (Cohen et al. [6]), flame propagation (Sivashinsky [35]), reaction diffusion combustion dynamics (Sivashinsky [36]), free surface film-flows (Benney [4], Sivashinsky and Michelson [37], Shlang and Sivashinsky [33], Hooper and Grimshaw [17]), and two-phase flows in cylindrical geometries (Frenkel et al. [13], Papageorgiou et al. [31]).

There have been numerous computational studies of (1.1) (Cohen et al. [6], Sivashinsky and Michelson [37], Aimar [1], Manneville [29], Frisch, She and Thual [14], Hyman and Nicolaenko [18], Hyman, Nicolaenko and Zaleski [19], Kevrekidis, Nicolaenko and Scovel [22], Greene and Kim [15] to mention a few), as well as analytical ones (Constantin et al. [8], Foias et al. [12], Babin and Vishik [3], etc.). The overall picture that emerges is that as the viscosity parameter ν is decreased, the large time behavior of the system varies from steady-state (for example *cellular*) solutions to complicated time-oscillatory (chaotic) ones. Such behavior has led to the conjecture that the solution behaves according to low modal dynamics with the determining number of Fourier modes being proportional to

$v^{-1/2}$ (i.e. Pomeau and Manneville [32]). Significant analytical results have provided estimates for the dimension and the nature of the global attractor (see [8],[12]), but the number of determining modes has not yet been estimated mathematically with satisfactory accuracy and thus we chose initially to integrate the partial differential equation directly rather than work with a truncated system. A truncated system of coupled nonlinear ODE's for the Fourier coefficients was also integrated and the number of determining coefficients was established experimentally. Since the dynamic behavior of the system is of a low modal structure (see earlier references), we found that all the important phenomena, for example period doubling cascades to chaos, are completely captured by a truncated system - this was verified by comparison of numerical solutions of the infinite dimensional dynamical system (PDE) and the truncated finite dimensional one, with emphasis on a window that yields a sequence of eight period doublings before chaos sets in. From hindsight we discovered that in the cases of the smaller values of v studied here, as many as approximately 40 coupled nonlinear equations must be retained if the time-periodic solutions are to be described with satisfactory accuracy.

Of particular relevance to the present work are the studies of Hyman and Nicolaenko [18] (also Hyman et al. [19], Kevrekides et al. [22], and Jolly et al. [20]). These studies are mostly concerned with the extensive numerical study of the related KS equation for the integral in space of our function $u(x,t)$. The equation used is

$$u_t + 4u_{xxx} + \alpha(u_{xx} + \tfrac{1}{2}u_x^2) = 0 \quad,$$

$$(x,t) \in R^1 \times R^+ \quad, \tag{1.2}$$

$$u(x,0) = u_0(x) \quad, \quad u(x+2\pi,t) = u(x,t) \quad.$$

The parameter α above is related to v by $\alpha = 4/v$. The range of α used was $4 \le \alpha \le 120$, which corresponds to $1/30 \le v \le 1$. Various attractors were constructed by changing the initial condition as well as α, by continuation methods where the initial condition is renormalized to its current value before α is changed. The bifurcation diagram reported contains windows of various attractors (fully modal, bimodal, trimodal and tetramodal fixed points) separated by oscillatory or chaotic orbits. A time-periodic orbit is reported in a small window $17.30 \le \alpha \le 22.50$.

The current study obtains a bifurcation diagram which is analogous to the above, but some essential differences must be pointed out. First of all, our concern is not with the full description of the inertial manifolds which are by no means easy to obtain since the initial conditions belong to an infinite-dimensional vector-space. Instead we want to investigate transition to chaos, which, as we have observed, occurs according to the classical routes of period-doubling bifurcations. Such

transitions to chaos have been described for iteration maps (Feigenbaum [10], Collet and Eckman [7], see Devaney [9] for a full description) as well as for low dimensional systems of ordinary differential equations such as the forced Duffing equation which is a second order system, and for the Lorenz attractor (see Guckenheimer and Holmes [16] and references therein). Numerical evidence of a period-doubling sequence has been presented by Knoblock et al. [23] and Lennie et al. [27] for the two-dimensional convection in a Boussinesq fluid. Many interesting results have also been found for the Ginzburg-Landau equation by Keefe [21] (see also Moon, Huerre and Redekopp [30], Sirovich and Rodriguez [35]) including a period-doubling sequence that supports an accurate estimate for the Feigenbaum number. Finally evidence of a period-doubling sequence has been discovered for a truncated model of the Kuramoto-Sivashinsky equation by Brown et al. [5] (see also Jolly et. al [20]); two period-doublings are reported in a window which corresponds to the tiny range $0.121223 \leq v \leq 0.121304$ for our problem. In the results we present here the initial condition is taken to be the same for all v. Global attractors are insensitive to such a choice, but in regimes where the solution becomes time-periodic and period-doubling bifurcations take place the present choice of initial condition enables both an accurate large-time integration as well as a quantification of the cascades (see later also). We emphasize here that in this article we exclude a complete study of the phase-space of initial conditions.

The structure of the paper is as follows. Section 2 describes the numerical methods used, while in Section 3 we begin to describe each window separately by showing representative numerical experiments in each case. Here we describe the first five windows which support solutions that are steady (i) (fully modal, bimodal, fully modal again, trimodal), time-periodic (ii), fully modal steady (iii), time-periodic again (iv) and steady tetramodal (v). In Section 4 results for the sixth window and beyond are given; the sixth window is time-periodic and contains a complete infinite sequence of period-doubling bifurcations leading to chaos. Results are presented for both a direct simulation (classical many mode discretization) and a truncated model (traditional Galerkin) with the low modal behavior of the dynamical system clearly brought out. The results are used to compute the Feigenbaum number for the cascade which is found to be in excellent agreement with Feigenbaum's universal theory. This Section also includes some preliminary results of solutions at smaller v showing the appearance of steady attractors of decreasing spatial period; time-periodicity and chaotic behavior persist as expected.

2. Numerical methods.

As mentioned earlier, our concern here is primarily with the numerical simulation of (1.1). Two numerical methodologies are used: A classical numerical discretization with many degrees of freedom (which we term the "direct" method) and a traditional Galerkin projection onto a low-dimensional inertial manifold that yields a coupled nonlinear system of ODE's to solve. In the former case we choose to perform the time integration by treating the linear part of the operator in Fourier space, and the nonlinear term in real space by a scheme that does not add numerical viscosity. This split step method maintains second order accuracy by the repeated application of the semi-groups, as suggested by the Strang split method. The time-step is chosen adaptively subject to several controls that ensure both numerical stability and high accuracy; the error in the experiments reported here is kept well below the 10^{-6} level. Such requirement is necessary to capture the nonlinear coupling of Fourier modes that are undergoing period-doubling cascades. For the Galerkin projection the Fourier coefficients were computed for a pre-determined dimension; a fourth order Runge-Kutta method was used to advance the nonlinear part in time, while the linear part was treated exactly by use of the split method described above together with repeated semi-group application that maintains overall accuracy. A natural accuracy test, throughout the computation, is the conservation of the spatial integral of u. The initial condition used is

$$u_0(x) = -\sin(x) \quad ,$$

and a consequence of this is that the integral over a spatial period vanishes for all time, and furthermore the solution maintains its odd parity. More generally, if the spatial profile of the solution is initially of the form

$$u(x,0) = \sum_{k \geq 1} a_k \sin kx \quad ,$$

then the mechanisms of the evolution of the partial differential equation respect this structure since,

$$u_{xx} + v\, u_{xxxx} = -\sum_{k \geq 1} (k^2 - vk^4)\, a_k \sin kx$$

and the nonlinear part becomes,

$$uu_x = (\tfrac{1}{2}u^2)_x = \tfrac{1}{2}\frac{d}{dx}(\sum_{k \geq 1} a_k \sin kx)^2 =$$

$$= \cdots = -\sum_{k \geq 1} (\tfrac{k}{2}(\sum_{\lambda \geq 1} a_{k+\lambda}a_\lambda - \tfrac{1}{2}\sum_{\lambda+\mu=k} a_\lambda a_\mu))\sin kx.$$

Thus the spatial profile remains a linear combination of sines for all times, i.e.

$$u(x,t) = \sum_{k \geq 1} a_k(t) \sin kx .$$

Due to the above observation the PDE (1.1) becomes equivalent to an infinite dimensional system of ordinary differential equations for $a_k's$, i.e.

$$a_k' = (k^2 - \nu k^4) a_k + \frac{k}{2} (\sum_{\lambda \geq 1} a_{k+\lambda} a_\lambda - \frac{1}{2} \sum_{\lambda + \mu = k} a_\lambda a_\mu) \quad \text{for } k \geq 1 . \tag{2.1}$$

The odd-parity property was utilized by a suitable filtering of Fourier coefficients; the filtering tolerance was set to a value between 10^{-10} and 10^{-12}. In the case of the direct computation the spatial discretizations were done on grids ranging from 128 to 1024 points. For windows other than the first steady attractor, at least 512 points were used. Results that are obtained by the projection method will be pointed out together with the number of modes retained for the dynamical system.

The results presented here were produced after several hundreds of numerical experiments which tracked the time evolution of the profile, its Fourier modes, its energy (L^2-norm) and the phase-plane of the energy and in some marginal cases of certain Fourier coefficients. The time evolution of the energy is very representative of the structure of the various attractors. Steady-state attractors evolve to a constant large-time state, while periodic or chaotic solutions have a time-oscillatory energy profile. Near window and subwindow (period-doubling) boundaries for the smaller values of ν at least, the time integration required as many as 200 time units (8×10^5 time steps) in order to sharply classify the ν-windows and subwindows. All periodic solutions reported here were derived by a phase-plane analysis of the data. As is described in the next Section many period-doubling bifurcations are evidenced from the phase-plane, which is used in conjunction with energy plots to build the geometrical structure of the solution in one time-period and so accurately estimate the the ν-position of the hyperbolic point corresponding to a period-doubling bifurcation, for example. Table 1 presents a summary of all windows discovered so far, together with sharp computed estimates of window boundaries.

3. Detailed numerical experiments. Pre-chaotic windows.

When the parameter ν decreases below unity, the solution undergoes its first Hopf bifurcation. In this Section we give a description of the dynamics in each of the first five windows.

(i) Steady attractors ,   .05985 $\leq \nu < 1$.

The main characteristic of this window, is the attraction of the initial profile to a steady-state. The steady-state is approached exponentially fast and is numerically achieved after a relatively short time

(5-10 time units in most cases). However the numerical convergence to the steady steady state is significantly delayed towards the lower end of the window where the first periodic attractor sets in. We subdivide the window into the following four subwindows :

(a) A fully modal steady attractor when $.248 \leq v < 1$.

(b) A bimodal steady attractor (i.e. where all the odd frequencies vanish) when $.0758 \leq v \leq .247$.

(c) Another fully modal steady attractor when $.06697 \leq v \leq .0758$.

(d) A trimodal steady attractor (where only the frequencies which are multiples of three survive) when $.05985 \leq v \leq .06695$.

For values of v near the lower boundary in fact, we find that there are about 30 modes which have an amplitude larger than 10^{-6}. In Figures (1.1), (1.2) and (1.3) we give sets of these attracting profiles for different decreasing values of v; Figures (1.1a) and (1.1b) cover ranges of v in the first subwindow. Figure (1.2a) covers a range of v at the lower end of the first subwindow as well as at the upper end of the second subwindow indicating a smooth transition from the fully modal first subwindow to the bimodal second subwindow. Figure (1.2b) also covers a range of v in the second subwindow, whereas figure (1.3a) covers a range in the third subwindow where the attracting profiles are trimodal. Comparison of figures (1.2b) and (1.3a) provides the indication that the transition of the attracting profiles between the two subwindows is smooth. Finally figure (1.3b) covers a range of values of v in the fourth and last subwindow where the attracting steady profiles are trimodal. The change in the shape of the limiting profiles in this subwindow is hardly visible, even though v changes "significantly" from .06695 to .06 . This is not surprising since under a similarity rescaling (see below) they correspond to fully modal steady profiles for v between .54 and .603 where not much change is observed either.

For values of v which are near 1, the profile is qualitatively similar to a sine wave. As v decreases, however, one more maximum and one more minimum are obtained after the profile attains an inflection at the anti-symmetry line $x = \pi$. Such solutions were also obtained by Frisch et al. [14] for values of v larger than or equal to 0.35; as a result of this they did not see profiles with four turning points. It is interesting at this point to describe an important property of the steady KS equation; if $u(x)$ is a solution corresponding to a viscosity v of the ODE obtained by dropping the time dependence in (1.1), then for any integer N there exists another solution $Nu(Nx)$ with viscosity v/N^2. Due to the periodic boundary conditions used here, N must be an integer. This self-similar property of the ordinary differential equation, satisfied by the steady states of the KS equation, permits the generation of a one parameter family of steady-states which grow in amplitude and decrease in period. In sub-

section (v), the tetramodal attractor, we give a numerical example of this self-similar property connecting steady-states for $N = 4$.

(ii) Time periodic attractors. $.055238 \leq v \leq .0599$.

The large time evolution of our initial value problem for v lying in the range covered by this window, is attraction to a time-periodic orbit. In all the results presented here, the period is defined for the energy (L^2-norm) of the solution. It is clear that the solution itself *can* have half the period of the energy but such a case was not observed when the Fourier coefficients were considered individually. Periodicity is determined by examination of the energy phase-plane (E versus dE/dt), and the period is evaluated from the evolution of the energy with time. All the solutions in this window are fully modal, and are characterized by a time-periodicity (the time period will be denoted by τ) which begins at a value of approximately $\tau = 1.0183$, increases slowly to $\tau = 1.18$ at a value of $v = .059$ and then doubles to $\tau = 2.374$ at a value of $v = .0559$. The doubling is instantaneous, in parameter space, and comes about by a slight disalignment of the maxima and minima of the energy-time graph. Some representative results from this window are given in Figures (2.1a,b)-(2.3a,b). The solution undergoes a period doubling as is evidenced by comparison of the phase-planes at $v = .057$ and $v = .0559$ - see Figures (2.1a), (2.2a). Figures (2.3a,b) correspond to $v = .0555$ and it can be seen that the 4-cycle property of the phase diagram is much more pronounced than at the slightly higher value of $v = .0559$; such drastic changes in the dynamics over small domains of the parameter space are typical and are encountered later on also. A summary of the results from this window is contained in Table 2.

(iii) Steady fully modal attractors. $.03965 \leq v \leq .055235$.

Here a new steady window is found with fully modal solutions which do not correspond to a rescaled value of the parameter v under the self-similar scaling described earlier. The new element here is the extremely slow convergence, still exponential nevertheless, towards the fixed point attractor. At such values of v the equations must be integrated to long times; this is to be expected since a straightforward perturbation analysis above the window-boundary yields a rate of decay of the distance (for example the L^2-norm) from the attractor, which is inversely proportional to the perturbation of v from the boundary. This is illustrated in Figures (3.1a)-(3.1c) for $v = .0397$. Figure (3.1a) shows the variation of the energy with time, while Figures (3.1b) and (3.1c) show the variation with time of the L^∞ norm and the L^∞ norm of the gradient of the solution respectively. It can be seen, that initially the solution passes through an oscillatory and almost periodic stage, and at a time of approximately 20 units its amplitude follows an envelope that takes the profile into the stationary attractor. In fact

during the oscillatory stage, the phase-plane of the energy is similar to that of the periodic window described next; once the steady-state begins its attraction the phase curve converges to a sink of course.

(iv) Time periodic attractors. $.03735 \le v \le .0396$.

Periodicity is again determined by examination of the energy phase-plane, and likewise the period is computed from the energy versus time plots. In this window the period begins at a value of approximately $\tau = .515$ when $v = .0396$, with a very slow convergence to the periodic attractor, and it increases smoothly, in parameter space, until it reaches the value $\tau = .684$ when $v = .03798$ with a much faster convergence to the the limit circle; the period then suddenly doubles to $\tau = 1.37$ at a value of $v = .03795$. As v is decreased further, the period undergoes a new slow increase to reach a value $\tau = 1.43$ at $v = .0377$; a small decrease of v to a value $.0376$ gives a new period doubling with $\tau = 2.87$. The period again increases slowly to a value $\tau = 3.0$ at $v = .03736$. At this point a slight decrease of v to the value $v = .037355$ gives a *period-halving* with the energy having a period $\tau = 1.5$. The last value of v computed in this window is $v = .03735$, for which the period is $\tau = 1.5$. The next numerical experiment with $v = .037345$ is outside this time-periodic window and yields a tetramodal steady-state (see later). These results are summarized in Table 3.

The results of Table 3 were obtained after numerous computations together with a careful examination of the oscillatory dynamics by means of phase-plane analysis, and representative solutions are given here. Some cases are described in full including the variation and phase-planes of certain Fourier modes, while other cases are described by the energy time series amid the energy phase-plane. These two plots are enough to conclude periodicity of solutions and their periods. In Figures (4.1a-d) we present results for $v = .038$ which is a representative parameter at the beginning of the window. These Figures show the variation of the energy with time, the energy phase-plane, and the phase planes of the first and tenth Fourier modes respectively; time periodicity of solutions is clear and we note that the Energy phase plane (Figure (4.1b)) is traced out 21 times since the time interval it depicts contains 21 periods. The time period of Fourier coefficients is the same as that for the energy, a fact that need not hold in general (see earlier comments); the reason it holds in the cases presented by this article, is that the actual solution $u(x,t)$ has a non-zero mean part in general.

As has been mentioned already (Table 3), a period-doubling takes place at $v = .03795$. This is evidenced very clearly in the phase-plane of the energy for this case which is given by Figure (4.2a). The phase-plane consists of two loops which are initially almost coincident (in fact they were coincident at $v = .038$) and this change produces the period-doubling. The corresponding energy variation

with time can be found in Figure (4.2b), from which the period is calculated to have a value of 1.37. The mechanism of the period doubling can also be seen from (4.2b), where every other wave crest and trough are reduced/increased slightly thus producing a phase-plane of index two and a period-doubling. We note also that there is no abrupt change in the wave-form that undergoes a period-doubling; only the value of the period doubles abruptly. Next we reduce the value of v by 5×10^{-5} to $v = .0379$. We are still in the same subwindow, but the phase plane diagram is now much more pronounced as Figure (4.3a) shows. The results for the last v from this subwindow is presented in Figures (4.3b), (4.3c) and (4.3d) which correspond to the phase-planes of the energy, the first and sixth Fourier coefficients respectively, at a value of $v = .0377$.

A reduction of v to the value .0376 brings us into a new subwindow with the solution undergoing a period doubling. Evidence for this can be found in Figure (4.4a) which depicts the phase-plane of the Energy at $v = .0376$; the time period is $\tau = 2.87$; Figures (4.4b) and (4.4c) are also given to show the evolution of the sixth Fourier coefficient with time and its corresponding phase-plane. The time-periodicity is again clear and similar results were found for all leading order (i.e. large enough for graphical purposes) Fourier coefficients. Such results are of course expected but they serve as a strict check on the numerical accuracy of the solutions so that we can confidently state that the time oscillations are by no means spurious, but in fact persist in a regular and accurate manner. The last case computed in this subwindow has $v = .03736$. The energy evolution and phase plane curves are given in Figures (4.5a) and (4.5b). The solution is just about to undergo a period halving and the index two property of the phase plane is only just discernible. A reduction of v to the value .037355 gave a period halving, and Figure (4.5c) shows the energy phase-plane for the last member of this window that was computed, $v = .03735$. . As expected, the mechanism that produced period-doublings is now working the opposite way to produce period-halvings (similar windows were also found by Knoblock et al. [23] for a convection problem). As mentioned earlier, a numerical experiment with $v = .037345$ produced a tetramodal steady-state which is representative of the window described next.

It is also interesting to observe the spatio-temporal evolution of the profiles, and we present this for two representative values of v from this window, $v = .039$ and .0375 respectively. The way this is done is by plotting on the same diagram the solution at successive increasing times. To make the evolution clearer the profiles are shifted vertically at each time interval producing pictures that capture the spatio-temporal evolution and in particular the time-periodicity of the solutions. Figure (4.6) corresponds to $v = .039$ while Figure (4.7) shows the results for $v = .0375$.

(v) <u>Steady tetramodal attractors.   .037348 ≤ v ≤ .0344.</u>

We present only one case (v = .0373) from this window since the results are qualitatively similar, the difference being in the final amplitude of the solution. For v = .0373, therefore, a steady-state is reached after approximately seven time units. The evolution of the energy is shown in Figure (5.1a) from which it is seen that after a few oscillations in time, the solution gets attracted to a tetramodal steady-state; this was determined from inspection of the Fourier coefficients. The corresponding profile at $t = 10$ is depicted in Figure (5.1b) which clearly shows the tetramodal character of the solution. This means that the solution is spatially periodic and of period π/2. Further more, this solution is obtainable from the self-similar re-scaling (see earlier) of the bimodal steady state at v = .1492 with the value of $N = 2$. This was checked and agreement is excellent.

4. Complete period-doubling cascade to chaos and computation of the Feigenbaum number.

(vi) <u>Time periodic attractors. Complete period–doubling sequence.   .0299756 ≤ v ≤ .0343.</u>

This window is to our view, the most important found in this work, and for this reason we concentrate on the results it produces rather than try to sharpen and classify the bifurcation diagram at higher values of the viscosity (the classification of the bifurcation diagram at high values of v has been the subject of extensive numerical and analytical studies by various authors - [18],[19], [20],[21]). The importance of this window is two-fold. First, it supports solutions that start as laminar steady-states (tetramodal waves) and then become time-periodic (this is also the case for window (iv) above). Second, the time-periods of the solution undergo a complete sequence of period-doubling bifurcations as the viscosity v is decreased, resulting in an accumulation point beyond which the solution is chaotic. Remarkably enough as many as 5 period-doubling bifurcations were accurately computed by the direct method and 8 period-doublings for the Galerkin procedure. This enables, for the first time, the accurate computation of the Feigenbaum number for the Kuramoto-Sivashinsky equation. Other investigations of PDE systems found results that were consistent with the universal Feigenbaum constant but no conclusive evidence was shown (see for example Knoblock et al. [22] for a convection problem, and Jolly et al. [20] for the KS equation). Significant results were obtained by Keefe [21], however, for the Ginzburg-Landau equation. After extensive numerical computations of even periodic solutions Keefe found a window containing a complete sequence of period-doubling bifurcations; the first five bifurcations were accurately obtained and based on the results the Feigenbaum number for the cascade was estimated to be approximately 4.4 to 4.7. The numerical method used in [21] was a pseudo-

spectral one with a 32 mode discretization. We mention here that these bifurcations take place on very small scales, in parameter space, and require a lot of care numerically, as well as an extensive computational effort towards a fairly sharp estimation of subwindow lengths (a subwindow should be understood to be a region in parameter space that separates period-doubling parameter values). We begin this section by presenting the results of the direct method by use of at least 512 Fourier modes. Most of the evidence from this approach is graphical and serves to show numerous period-doublings through phase-plane analysis. We also re-computed this same window by means of a truncated model that retains the leading 36 Fourier modes. The results of the two methods agree to at least 4 decimal places (by results here we mean the positions in v-space of the various subwindows); a quantitative analysis of the results obtained from the 36-mode Galerkin expansion enables the accurate computation of the universal Feigenbaum number of the cascade (see later for details).

The direct computation of the PDE provides results for the first six subwindows over which the solution attains five period-doublings. Improvement to a sixth period-doubling would require a substantial amount of computational resources and is wise at this point to turn to finite-dimensional versions of the equations. For example computations that retain 36 Fourier modes are in general at least 8 times faster than direct computations; in the absence of sharp-analytical results direct computations are essential in gauging the accuracy or sufficiency of truncated models. As mentioned already, 36 modes are capable of capturing a complete set of period-doubling bifurcations that precede chaos, and more importantly are in complete agreement with the Feigenbaum universal constant. To give an example of the numerical restrictions that are present in either direct or finite-dimensional approaches, our direct numerical solutions for $v = .0299756$ gave a time periodic solution with $\tau = 7.04$ while at $v = .02997$ the solutions appear to be chaotic. In a distance of less than 5.6×10^{-5}, therefore, numerous period-doubling bifurcations take place (to conjecture an infinite number would be too hasty because the *chaotic* solution at $v = .02997$ can be thought of as an oscillatory solution with a very large period; the period is so large that discourages any attempt at its numerical computation). It can be seen, therefore, that we would very soon run out of computational accuracy, since subwindow lengths would be of the same order as computer round-off error. We decided, therefore, to concentrate on the first five subwindows (eight for the 36 mode model) and compute the Feigenbaum number from these.

For brevity of the description we will restrict our presentation to phase-plane curves of the energy. Each case presented was computed with 512 Fourier modes and approximately 4×10^4 time steps (a run takes about 20 minutes CPU time on a CRAY-II and about 4 hours CPU time on a SPARC work-station; all runs use double precision). Accuracy tests were also made for many runs by use of 1024 Fourier modes; all results reported here are insensitive to such refinements as the truncated

system also shows (see later). We give representative results from each subwindow and show the behavior near subwindow boundaries. The steady tetramodal solution gets attracted to a time-periodic orbit when v is reduced below a value of .0345. The phase-plane of the L^2-norm of the solution is a 1-cycle initially. In Figure (6.1a) the phase plane for $v = .0342$ is shown over a time interval from 1.0 to 34.5. It is clear that the solution gets attracted to a time-periodic orbit of index 1; the period is 0.37. As v is decreased the period increases smoothly and the 1-cycle topology of the phase-plane persists until the first period doubling suddenly appears at a value of v just above .0304. The phase-plane corresponding to $v = .0304$ is not shown because the period-doubling bifurcation has just taken place and within graphical accuracy the phase-plane appears to have the same topology as in the previous subwindow. Careful inspection of the left side of the curve, however, shows that there are two distinct branches; the period of the solution is 0.89. The two branches begin to move apart as v decreases further. An example of this change in the phase-plane, which in turn corresponds to a change in the oscillatory structure of the solution, is seen in Figures (6.1b-c); the value of v is .0303 and the period is the same as before, $\tau = 0.89$. The last picture we present from this subwindow is Figure (6.1d) for a value $v = .03007$. The characteristics of the time oscillations are qualitatively the same as before with the two loops well separated and with time-period $\tau = 0.88$.

We next decrease the value of v slightly. A new subwindow is found which develops after a period-doubling bifurcation at a value of v between .03007 and .030065. The phase-plane curve now becomes a 4-cycle and in one complete time oscillation the energy has eight turning points, four of which are maxima and four minima. A characteristic phase-plane curve for bifurcation parameters near the upper edge of the second subwindow, is Figure (6.2a) which has $v = .03006$; the time-period is $\tau = 1.76$. The index 4 property is evident and appears by a slight disalignment of the phase plane branches. We also note that at this value of v the maxima of the energy are noticeably different whereas the minima are almost indistinguishable. Other cases from this subwindow are also given in Figures (6.2b-d). The value of the viscosity is $v = .030015$, $.03$, $.029998$ respectively. The period is 1.76 and the 4-cycle property, characteristic of this subwindow, is very clear. Figure (6.2d), which has $v = .029998$ is at the lower edge of the second subwindow and is representative of the dynamics just before a second period-doubling bifurcation.

Next the value of v was decreased to .0299975; at first sight this v seems to belong to the second subwindow but a careful inspection of one of the loops shows that a period-doubling takes place somewhere between $v = .029998$ and .0299975 leading to an estimated time-period of $\tau = 3.52$ and phase-plane characteristics for this subwindow of index 8. For smaller values of v the phase-plane loops begin to drift apart. Figures (6.3a-c) show a sequence of energy phase-plane diagrams for three

decreasing values of v that belong to this third subwindow; these values are $v = .029995$, $.02999$, $.0299815$. The last computation in this subwindow is at $v = .0299815$ and the period is $\tau = 3.52$.

The next numerical experiment has $v = .029981$. Once more, careful inspection of the phase-plane shows that a 16-cycle is obtained and hence another period-doubling bifurcation takes place somewhere between $v = .0299815$ and $.029981$. To see this one must concentrate, for example, on that region of the phase plane described by $17.5 < E < 18$ and dE/dt near zero. Before the period-doubling bifurcation takes place there is a single branch traced out in the phase-plane while now two branches are distinguishable within the limits of graphical accuracy. At smaller values of v the branches move apart and the 16-cycle property is very clearly seen. Figures (6.4a-c) give representative phase-planes corresponding to a sequence of viscosities which span this fifth subwindow. The bifurcation parameters are $v = .02998$, $.029978$, $.0299756$ respectively. The value $v = .0299756$ is also the last computation from this subwindow; the period is $\tau = 7.04$.

In Figures (6.5a-d) we present results after another period-doubling occurs. The first case, Figure (6.5a), has $v = .029975$ and the phase-plane appears to be a 32-cycle with a period of at least 14.0. The complexity of the dynamics becomes more enhanced as v is decreased even further, and it becomes very difficult and computationally expensive to try and follow more period-doubling bifurcations than the ones described here. Figures (6.5b-d) give a flavor of the complicated dynamics that one has to resolve, for the values $v = .02997$, $.02995$, $.0299$ respectively.

Computation of the Feigenbaum number.

As mentioned earlier, the results we have from the direct numerical simulation are probably not extensive enough for an *accurate* determination of the Feigenbaum number. The lacking ingredient is the sharp estimation of subwindow boundaries which take on a central role in such a computation. As a result of this, a straightforward calculation of the ratio of successive subwindow lengths suffers from certain inaccuracies. For completeness, however, we give the results and stress that they can be improved by resort to a much more extensive numerical search. If we label the lengths of successive subwindows by l_i , $i=1,\infty$ then the following ratios are obtained from the results of Table 4 : $l_2/l_1 = 5.42$, $l_3/l_2 = 11.35$ and $l_4/l_3 = 2.77$. The cascade is still in its early stages but the distance, in v-space, of the fourth subwindow lower boundary from the point where the strange attractor seems to commence, is of the order of 10^{-6}. Due to the non-sharp classification of the subwindows, the ratios are only of the same order of magnitude as the universal Feigenbaum constant. Our data is much more extensive for the 36-mode Galerkin approach and they yield excellent results as we explain next.

The period-doubling route to chaos is well documented for certain low dimensional models (see earlier references), but it is believed that the Feigenbaum constant, originally found for iteration maps, is universal and appears in other high-dimensional systems also. In what follows we present numerical evidence of this universality for the Kuramoto-Sivashinsky equation. Suppose that period-doublings take place at some successive values, v_n say, of the viscosity parameter. The theory predicts an accumulation of such bifurcation points as $n \rightarrow \infty$ and in fact the universal constant is given by :

$$\lim_{n \rightarrow \infty} \left[\frac{v_n - v_{n-1}}{v_{n+1} - v_n} \right] = 4.6692016... \quad .$$

The obvious way to test our results against the theory is to form the successive ratios indicated above, for our computed subwindow boundaries. The results of this approach are given in Table 5. The first column of the Table gives our estimate for subwindow boundaries (for example the first two numbers in the first column show the beginning and end respectively of the first periodic subwindow; the second and third numbers indicate the beginning and end of the second periodic subwindow etc.), the second column shows the subwindow length and the third column contains the ratio of successive subwindow lengths. Note that the cascade develops as we move down the Table and by the time the third period-doubling bifurcation is attained the geometric ratio of successive bifurcation points is 4.27, a number already close to Feigenbaum's universal constant. It is worth noting that subwindow lengths are shrinking significantly and the last subwindow that was computed accurately had a length of 1.3×10^{-7}. It is clear, therefore, that the difficulty of the numerical experiments increases as the cascade develops and some special continuation algorithms were used towards the expediency of our estimates. Such accuracy measures are essential in the production of four successive bifurcation ratios from the fourth to the eighth subwindow, which are at an error of at most 4% from the universal constant of 4.669201609... . Various other tests can also be performed using the data. For example we can pick a subwindow which begins at v_n and which has length l_n. Then by use of the *computed* accumulation point $v_c = .029969275$ and by assumption of an infinite cascade, it is easy to show that there exists a geometric ratio

$$\frac{1}{\delta} = 1 - \frac{l_n}{v_n - v_c} \quad ,$$

which takes the point v_n to the accumulation point v_c. The number δ above, provides then the "Feigenbaum number" for the chosen subwindow. The theory tells us that as the value of v_n is chosen to be progressively closer to the accumulation point, δ then converges to the universal constant. This version of the cascade theory was also applied to our numerical data. The results are similar to those in

Table 5 but they are slightly more accurate; the gain in accuracy is due to elimination of combination of errors that a successive ratio inevitably contains. Finally, we also computed the Feigenbaum number, based on subwindows which are not successive but have a factor of 4 difference in their time-periods. A ratio is again obtained whose square root should converge to the universal constant after an infinite number of bifurcations. After eight bifurcation (even less in fact) the numbers obtained are again very similar to those of Table 5 and we omit further details here.

Finally in this Section we present a brief summary of some of the results obtained for values of v which take the dynamics beyond the complete sequence of period-doubling bifurcations just described. The richness of the attractors is highly enhanced and the regions in parameter-space over which changes take place become smaller. In this article we choose to describe three additional windows; these are the chaotic window entered immediately after the period-doublings described above, the second is a time-periodic attractor, and the third is a region of parameter space that supports chaotic, steady and time-periodic solutions.

(vii) Window of Chaotic Trajectories. $.0252 \le v \le .029755$.

No recognizable patterns are observed either in the energy time series or in the phase planes for values of the parameter in this window. It should be noted, however, that all the plotted quantities remain bounded in agreement with the theory (Constantin et al [8].) See figures (7.1a-d).

(viii) Time periodic attractors. $0.023 \le v \le 0.0251$.

Another window with time-periodic attractors and at least three period-doubling bifurcations was also found. Unlike the previous periodic window the period starts with small values at the end of the window - the period at $v = 0.023$ is $\tau = .26$ - and reaches the value $\tau = 2.86$ at $v = 0.0251$ after three period doublings. The results from this window are summarized in Figures (8.1a-c) for a representative member $v = .025$.

(ix) Window of Chaotic Trajectories. $? \le v \le 0.0225$.

Chaotic solutions are also found in this subwindow with no recognizable patterns to report. The ambiguity of the lower bound of this window remains unresolved due to the computational cost of the required runs but also due to the well-known fact that this is not the last chaotic window to be found. Window and subwindow lengths become vanishingly smaller thus halting any rational numerical progress. The discovery of various attractors becomes a hit or miss problem and, for example, in the range $.008 \le v \le .0225$ we managed to find a strange attractor $(v = .0225)$, a time-periodic attractor $(v = .017)$, and bimodal steady attractor $(v = .015)$ before another strange attractor is obtained at $v = .008$. These results are summarized in Figures (9.1a-e). For graphical clarity, the phase-planes in

this set of Figures were obtained by plotting (E , dE/dt) pairs which are separated by a time which is a large multiple of the time-step.

5. Conclusions.

We have carried out an extensive numerical study of the Kuramoto-Sivashinsky equation. Our emphasis is on the characterization of transition to chaos and we restricted ourselves to odd-parity solutions derived from the same initial conditions and which are easily reproducible by a single computer run. The results for large values of the parameter v, i.e. before chaos or multiple period-doubling bifurcations, are completely in line with those of previous investigators (see Introduction). The new behavior we found, and which to our knowledge has not been reported before for the Kuramoto-Sivashinsky equation, is the computation of several windows which support time-periodic orbits and which themselves contain other subwindows which are separated by period-doubling bifurcations in parameter space. The third periodic window we found (see Section 4 above) provides substantial numerical evidence of a complete sequence of period-doubling bifurcations before chaos sets in. Based on our numerical solutions we computed the Feigenbaum number following the first eight bifurcations of the cascade, and found excellent agreement with Feigenbaum's universal constant.

Acknowledgements.

6. Bibliography.

[1] Aïmar, M.T., *Etude numérique d'une équation dévolution non linéaire dérivant l'instabilité thermodiffusive d'un front de flamme*, Thèse Troisième cycle Université de Province (1982).

[2] Babchin, A.J., Frenkel, A.L., Levich, B.G., Sivashinsky, G.I., *Nonlinear Saturation of Rayleigh-Taylor Instability in thin films*, Phys. Fluids 26 (1983), pp. 3159-3161.

[3] Babin, A.V., Vishik, M.I., *Regular attractors and semi-groups of evolution equations*, J. Math. Pures Appl., vol. 62 (1983) pp. 441-491.

[4] Benney, D.J., *Long Waves in Liquid films*, J. Math. & Phys. 45 (1966), pp. 150-155.

[5] Brown, H., S., Jolly, M.S., Kevrekidis, I.G., Titi, E.S., *Use of Approximate Inertial Manifolds in Bifurcation Calculations*, Proc. NATO Adv. Res. Workshop on : Continuation and Bifurcations : Numerical Techniques and Applications, 18-22 September, 1989, Leuven, Belgium.

[6] Cohen, B.I., Krommes, J.A., Tang, W.M., Rosenbluth, M.N., *Non-linear saturation of the dissipative trapped ion mode by mode coupling*, Nucl. Fusion, vol. 16, (1976) pp. 971-992.

[7] Collet, P., Eckman, J.P., *Iterated maps of the Interval as Dynamical Systems*, Birkhauser, Boston, 1980.

[8] Constantin, P., Foias, C., Nicolaenko, B., Temam, R., *Integral Manifolds and Inertial Manifolds for Dissipative Partial Differential Equations*, Appl. Math. Sciences, No. 70, Springer-Verlag, New York, 1988.

[9] Devaney, R.L., *An Introduction to Chaotic Dynamical Systems*, Benjamin/Cummings, Menlo Park, Ca., 1986.

[10] Feigenbaum, M., *The onset spectrum of turbulence*, Phys. Lett., vol. 74B, pp. 375-378.

[11] Feigenbaum, M., *The transition to aperiodic behavior in turbulent systems*, Commun. Math. Phys., vol. 77 (1980), pp. 65-86.

[12] Foias, C., Jolly, M.S., Kevrekidis, I.G., Sell, G.R., Titi, E.S., *On the Computation of Inertial Manifolds*, Phys. Lett. A, Vol. 131, number 7,8 (1988).

[13] Frenkel, A.L., Babchin, A.J., Levich, B.G., Shlang, T., Sivashinsky, G.I., J. Colloid. Interface Sci., vol. 115 (1987) pp. 225.

[14] Frisch, U., She, Z.S., Thual, O., *Viscoelastic behaviour of cellular solutions to the Kuramoto-Sivashinsky model*, J. Fluid Mech., vol. 168 (1986) pp. 221-240.

[15] Greene, J.M., Kim, J.-S., *The steady states of Kuramoto-Sivashinsky equation*, Physica D, vol. 33 (1988) pp. 99-120.

[16] Guckenheimer, J., Holmes, P., *Nonlinear Oscillations, Dynamical Systems and Bifurcations of Vector Fields*, Springer-Verlag, New York, 1984.

[17] Hooper, A.P., Grimshaw, R., *Nonlinear instability at the interface between two fluids*, Phys. Fluids, vol. 28 (1985) pp. 37-45.

[18] Hyman, J.M., Nicolaenko, B., *The Kuramoto-Sivashinsky equations, a bridge between PDEs and dynamical systems*, Physica D, vol. 23 (1986), pp. 113-126.

[19] Hyman, J.M., Nicolaenko, B., Zaleski, S., *Order and complexity in the Kuramoto-Sivashinsky model of turbulent interfaces*, Physica D, vol. 23 (1986), pp. 265-292.

[20] Jolly, M.S., Kevrekides, I.G. and Titi, E.S., *Approximate inertial manifolds for the Kuramoto-Sivashinsky equation: analysis and computations*, Physica D, vol. 44 (1990) pp. 38-60.

[21] Keefe, L.R., *Dynamics of perturbed wavetrain solutions to the Ginzburg-Landau equation*, Stud. Appl. Math., vol. 73 (1985), pp. 91-153.

[22] Kevrekidis, I.G., Nicolaenko, B., Scovel, C., *Back in the saddle again : A computer assisted study of Kuramoto-Sivashinsky equation*, SIAM J. Appl. Math., vol. 50, No. 3 (1990) pp. 760-790.

[23] Knoblock, E., Moore, D.R., Toomre, J., Weiss, N.O., *Transitions to chaos in two-dimensional double-diffusive convection*, J. Fluid Mech., vol. 166 (1986) pp. 409-448.

[24] Kuramoto, Y., *Diffusion-induced chaos in reactions systems*, Suppl. Prog. Theor. Phys., vol. 64 (1978) pp. 346-367.

[25] Kuramoto, Y., Tsuzuki, T., *On the formation of dissipative structures in reaction-diffusion systems*, Prog. Theor. Phys., vol. 54 (1975) pp. 687-699.

[26] Kuramoto, Y., Tsuzuki, T., *Persistent propagation of concentration waves in dissipative media far from thermal equilibrium*, Prog. Theor. Phys., vol. 55 (1976) pp. 356-369.

[27] Lennie, T.B., McKenzie, D.P., Moore, D.R., Weiss, N.O., *The breakdown of steady convection*, J. Fluid Mech., vol. 188 (1988) pp. 47-85.

[28] Lin, S.P., *Finite Amplitude Side-Band Stability of Viscous Fluid*, J. Fluid Mech., vol. 63 (1974) pp. 417-429.

[29] Manneville, P., *Lyapunov Exponents for the Kuramoto-Sivashinsky Equations*, Proc. Conf. on Turbulence, Nice 1984, Springer-Verlag Lecture Notes in Physics, New York (1985).

[30] Moon, H.T., Huerre, P., Redekopp, L/G., *Transitions to chaos in the Ginzburg-Landau equation*, Physica D, vol. 7 (1983), pp. 135-150.

[31] Papageorgiou, D.T., Maldarelli, C., Rumschitzki, D.S., *Nonlinear interfacial stability of core-annular film flow*, Phys. Fluids A, vol. 2, No. 3 (1990) pp. 340-352.

[32] Pomeau, Y., Manneville, P., *Intermittent transition to turbulence in dissipative dynamical systems*, Commun. Math. Phys., vol. 74 (1980) pp. 189-197.

[33] Pumir, A., Manneville, P., Pomeau, Y., *On solitary waves running down an inclined plane*, J. Fluid Mech., vol. 135 (1983) pp. 27-50.

[34] Shlang, T., Sivashinsky, G.I., *Irregular flow of a liquid film down a vertical column*, J. Phys., vol. 43, (1982) pp. 459-466.

[35] Sirovich, L., Rodriguez, J.D., *Coherent Structures and Chaos : A Model Problem*, Phys. Lett., vol. 120, No. 5 (1987) pp. 211-214.

[36] Sivashinsky, G.I., *Nonlinear analysis of hydrodynamic instability in laminar flames, Part I. Derivation of basic equations*, Acta Astronautica, vol. 4 (1977) pp. 1176-1206.

[37] Sivashinsky, G.I., *On flame propagation under conditions of stoichiometry*, SIAM J. Appl. Math., vol. 39 (1980) pp. 67-82.

[38] Sivashinsky, G.I., Michelson, D.M., *On irregular wavy flow of a liquid down a vertical plane*, Prog. Theor. Phys. 63 (1980) 2112-2114.

[39] Temam, R., *Infinite-dimensional Dynamical Systems in Mechanics and Physics*, Springer-Verlag, New York, 1988.

7. Tables.

Overview of the attracting manifolds				Description of the attractors
	Window range			Description of the attractors
1	≤	v	< ∞	Constant states.
.2475	≤	v	< 1	Fully modal steady attractors.
.0756	≤	v	≤ .2472	Bimodal steady attractors.
.06697	≤	v	≤ .0755	Fully modal steady attractors.
.0599	≤	v	≤ .06695	Trimodal steady attractors.
.055238	≤	v	≤ .05985	Periodic attractors.
.03965	≤	v	≤ .055235	Fully modal steady attractors.
.03735	≤	v	≤ .0396	Periodic attractors.
.0344	≤	v	≤ .037348	Tetramodal steady attractors.
.029756	≤	v	≤ .0343	Periodic attractors. Complete period-doubling sequence towards v=.029756.
.0252	≤	v	≤ .029755	Chaotic oscillations.
.024	≤	v	≤ .0251	Periodic attractors. Complete period-doubling sequence towards v=.02512.
?	≤	v	≤ 0.023	Chaotic oscillations.

Table 1

First Periodic Window .0598 $\leq$ v $\leq$ .055238		
Viscosity v	**Period** τ	**Figures**
.0598	1.018	
.0595	1.03	
.059	1.05	
.058	1.08	
.057	1.13	(2.1a,b)
.056	1.18	
.0559	1.183	(2.2a,b)
.05585	2.374	
.0555	2.48	(2.3a,b)
.0553	2.59	
.05525	2.663	
.05524	2.729	

Table 2

Second Periodic Window $.03735 \leq v \leq .0396$		
Viscosity v	Period τ	Figures
.0396	0.515	
.03955	0.533	
.0395	0.53	
.0393	0.55	
.039	0.59	
.038	0.68	(4.1a-d)
.03798	0.684	
.03795	1.37	(4.2a,b)
.0379	1.38	(4.3a)
.0378	1.40	
.0377	1.43	(4.3b-d)
.0376	2.87	(4.4a-d)
.0375	2.95	
.0374	3.00	
.03738	3.00	
.03736	3.01	(4.5a,b)
.037355	1.51	
.03735	1.51	(4.5c)

Table 3

Third Periodic Window .0343 ≤ v ≤ .0299756		
Viscosity v	**Period τ**	**Figures**
.0343	.368	
.0342	.37	(6.1a)
.032	.44	
.0304	.89	
.0303	.89	(6.1b,c)
.03007	.88	(6.1d)
.030065	1.76	
.03006	1.76	(6.2a)
.030015	1.76	(6.2b)
.03	1.76	(6.2c)
.029998	1.76	(6.2d)
.0299975	3.52	
.029995	3.52	(6.3a)
.02999	3.52	(6.3b)
.029985	3.52	
.029983	3.52	
.0299815	3.52	(6.3c)
.029981	7.04	
.02998	7.04	(6.4a)
.029979	7.04	
.029978	7.04	(6.4b)
.029976	7.04	
.0299758	7.04	
.0299756	7.04	(6.4c)
.029975	14.08	(6.5a)

Table 4

36-mode Galerkin Expansion		
Subwindow boundary	Length	Ratio
.034615		
.0303175	.0042975	
.0300494	.0002681	16.0295
.02998665	.00006275	4.27
.029973005	1.3645×10^{-5}	4.6
.02997007	2.935×10^{-6}	4.65
.029969435	6.35×10^{-7}	4.62
.029969305	1.3×10^{-7}	4.88

Table 5

8. Figures

Figure (1.1) : Steady attracting modal profiles :

    (a) $v = .6\ .7\ .8\ .9$.

    (b) $v^\sim =^\sim .26\ .28\ .3\ .35\ .4\ .5$.

Figure (1.2) : Steady attracting profiles :

    (a) $v = .2\ .22\ .24\ .248\ .28$.

    (b) $v = .08\ .09\ .12\ .15\ .2$.

Figure (1.3) : Steady attracting trimodal profiles :

    (a) $v = .067\ .07\ .072\ .074\ .0755\ .08$.

    (b) $v = .06\ .061\ .063\ .065\ .06695$.

Figure (2.1) : First periodic window, $.0598 \le v \le .055238$:

    (a) Phase plane of Energy - $v = .057$.

    (b) Energy time series - $v = .057$.

Figure (2.2) : First time-periodic window, $.0598 \le v \le .055238$:

    (a) Phase plane of Energy - $v = .0559$.

    (b) Energy time series - $v = .0559$.

Figure (2.3) : First time-periodic window, $.0598 \le v \le .055238$:

    (a) Phase plane of Energy - $v = .0555$.

    (b) Energy time series - $v = .0555$.

Figure (3.1) : Window (iii), fully modal steady attractors, $.06697 \le v \le .0755$:

    (a) Energy against time - $v = .0397$.

    (b) Supremum of $u(x,t)$ against time - $v = .0397$.

    (c) Supremum of d/dx of $u(x,t)$ against time - $v = .0397$.

Figure (4.1) : Second periodic window, time-period $\tau = .68$:

    (a) Energy against time - $v = .038$.

    (b) Phase plane of Energy - $v = .038$.

    (c) First Fourier coefficient against time - $v = .038$.

    (d) Tenth Fourier coefficient against time - $v = .038$.

Figure (4.2) : Second periodic window, time-period $\tau = 1.37$:

    (a) Phase plane of Energy - $v = .03795$.

    (b) Energy time series - $v = .03795$.

Figure (4.3) : Second periodic window, time-period $\tau = 1.37$ to 1.43 :

    (a) Phase plane of Energy - $v = .0379$.

    (b) Phase plane of Energy - $v = .0377$.

    (c) Phase plane of the first Fourier coefficient - $v = .0377$.

    (d) Phase plane of the sixth Fourier coefficient - $v = .0377$.

Figure (4.4) : Second periodic window, time-period $\tau = 2.87$:

(a) Phase plane of Energy - $v = .0376$.

(b) Time series of sixth Fourier coefficient - $v = .0376$.

(c) Phase plane of the sixth Fourier coefficient - $v = .0376$.

Figure (4.5) : Second periodic window, period-halving from $\tau = 3.01$ to 1.51 :

(a) Energy time series - $v = .03736$.

Phase plane of Energy - $v = .03736$.

Phase plane of Energy - $v = .03735$.

Figure (4.6) : Second periodic window :

Evolution of the spatial profile in the periodic attractor - $v = .039$.

Figure (4.7) : Second periodic window :

Evolution of the spatial profile in the periodic attractor - $v = .0375$.

Figure (5.1) : Window (v), steady tetramodal attractors, $.0344 \leq v < .037348$:

(a) Energy time series - $v = .0373$.

(b) Steady tetramodal attracting profile - $v = .0373$.

Figure (6.1) : Third periodic window, first period-doubling :

(a) Phase plane of Energy - $v = .0342$.

(b) Phase plane of Energy - $v = .0303$.

(c) Energy time series - $v = .0303$.

(d) Phase plane of Energy - $v = .03007$.

Figure (6.2) : Third periodic window, second period-doubling :

(a) Phase plane of Energy - $v = .03006$.

(b) Phase plane of Energy - $v = .030015$.

(c) Phase plane of Energy - $v = .03$.

(d) Phase plane of Energy - $v = .029998$.

Figure (6.3) : Third periodic window, third period-doubling :

(a) Phase plane of Energy - $v = .029995$.

(b) Phase plane of Energy - $v = .02999$.

(c) Phase plane of Energy - $v = .0299815$.

Figure (6.4) : Third periodic window, fourth period-doubling :

(a) Phase plane of Energy - $v = .02998$.

(b) Phase plane of Energy - $v = .029978$.

(c) Phase plane of Energy - $v = .0299756$.

Figure (6.5) : Third periodic window, fifth period-doubling :

(a) Phase plane of Energy - $v = .029975$.

(b) Phase plane of Energy - $v = .02997$.

(c) Phase plane of Energy - $v = .02995$.

(d) Phase plane of Energy - $v = .0299$.

Figure (7.1) : Chaotic windows, $.0252 \leq v \leq .029755$:

(a) Energy time series (Chaotic case) - $v = .028$.

(b) Energy time series (Chaotic case) - $v = .027$.

(c) Energy time series (Chaotic case) - $v = .0255$.

(d) Energy time series (Chaotic case) - $v = .0252$.

Figure (8.1) : Time-periodic attractors, $.023 \leq v \leq .0251$:

(a) Energy time series (Periodic case) - $v = .025$.

(b) Energy time series (Blow-up) - $v = .025$.

(c) Phase plane of Energy - $v = .025$.

Figure (9.1) : Chaotic windows, $? \leq v \leq .0255$:

(a) Phase plane of Energy (Chaotic case) - $v = .0225$.

(b) Phase plane of Energy (Periodic case) - $v = .017$.

(c) Energy time series (Periodic case) - $v = .017$.

(d) Energy time series (Bimodal steady attractor) - $v = .015$.

(e) Phase plane of Energy (Chaotic case) - $v = .008$.

.

Figure (1.1)

Steady attracting profile — ν= .6 .7 .8 .9

(a)

Diamond=.6 Octagon=.7 Triangle=.8 Square=.9
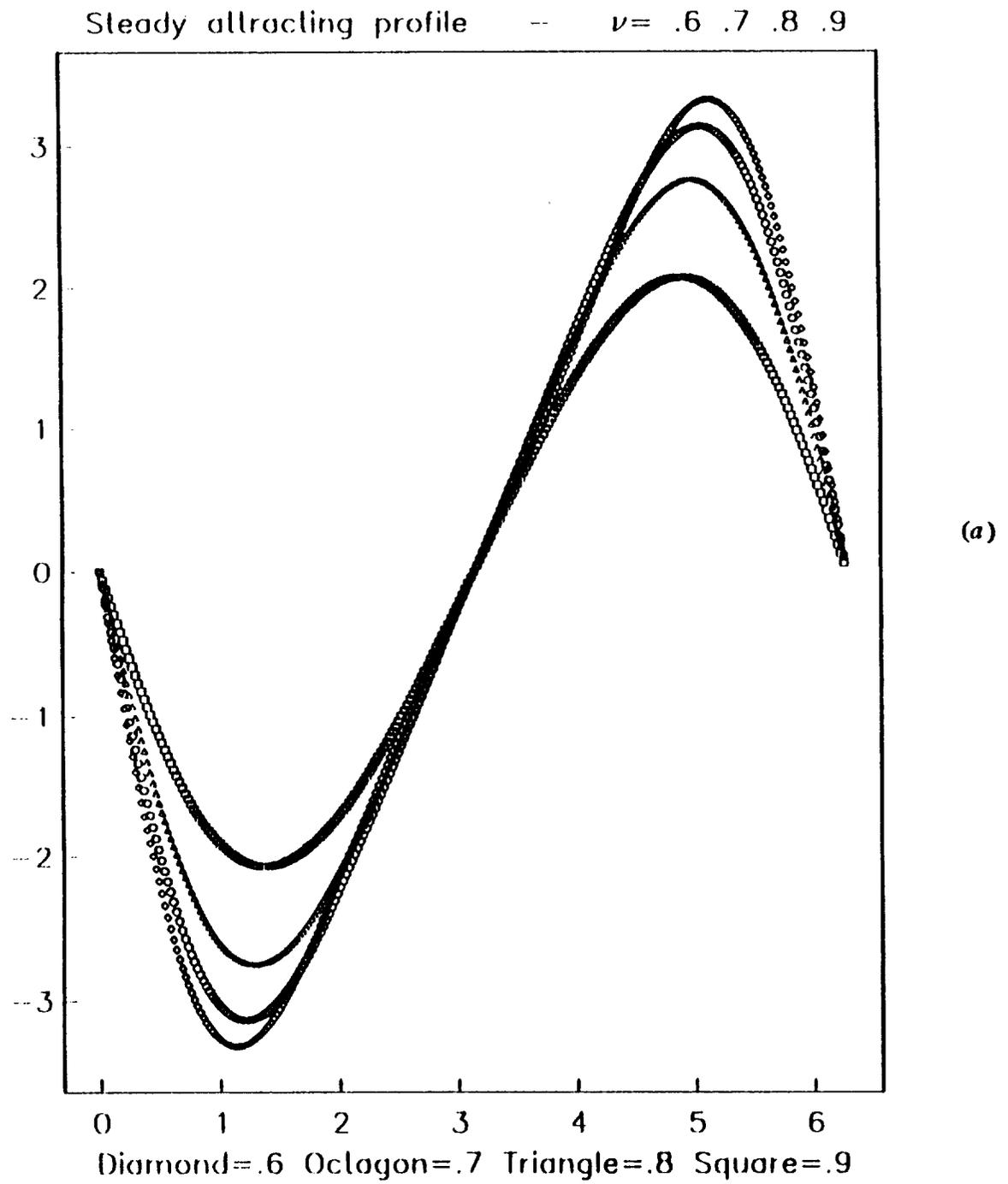
Steady attracting profiles — $\nu = .26\ .28\ .3\ .35\ .4\ .5$
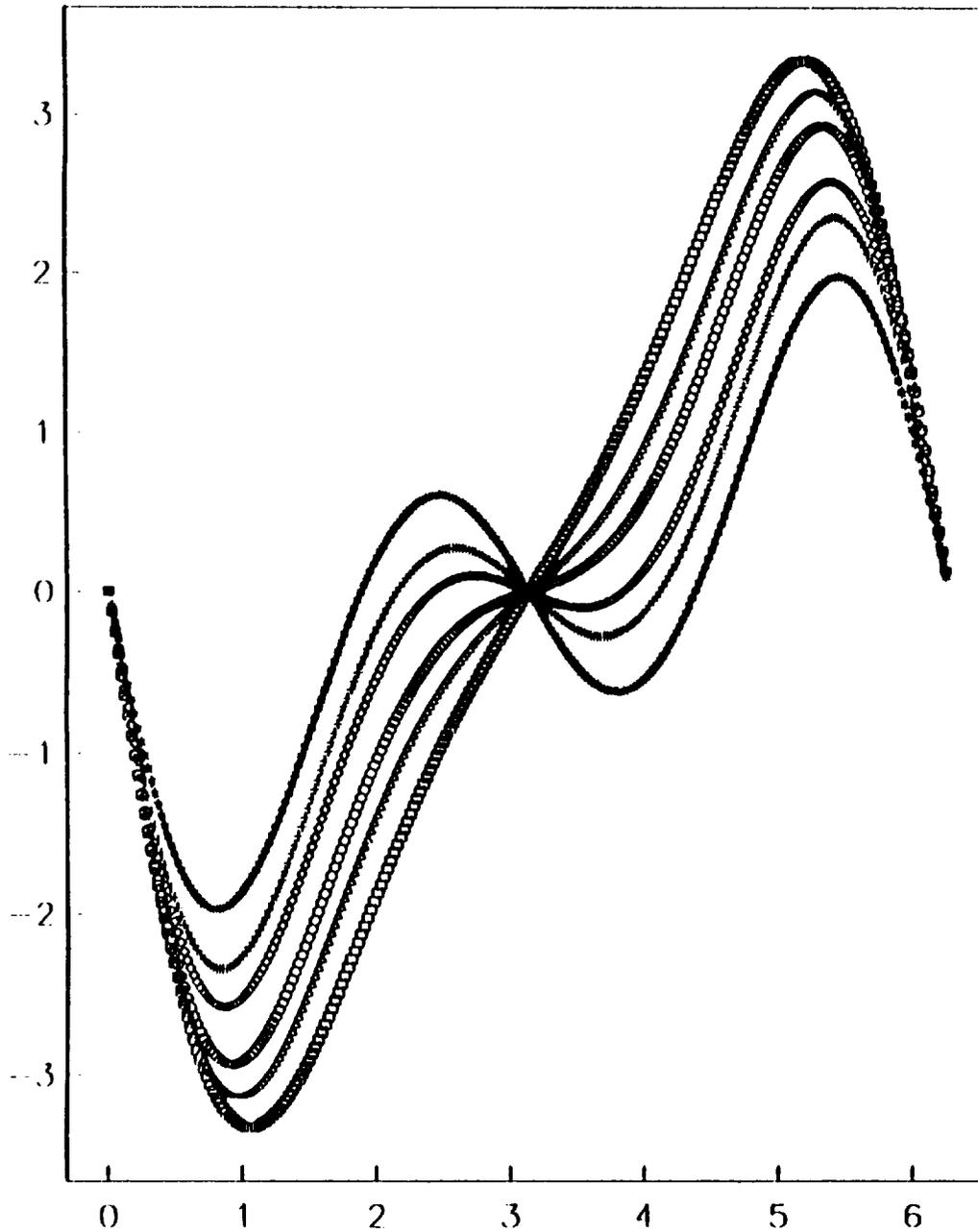
(b)

Asterisk=.26 Plus=.28 Diamond=.3 Octagon=.35 Triangle=.4 Square=.5

Figure (1.2)

Steady attracting profiles   -- ν= .2 .22 .24 .248 .28
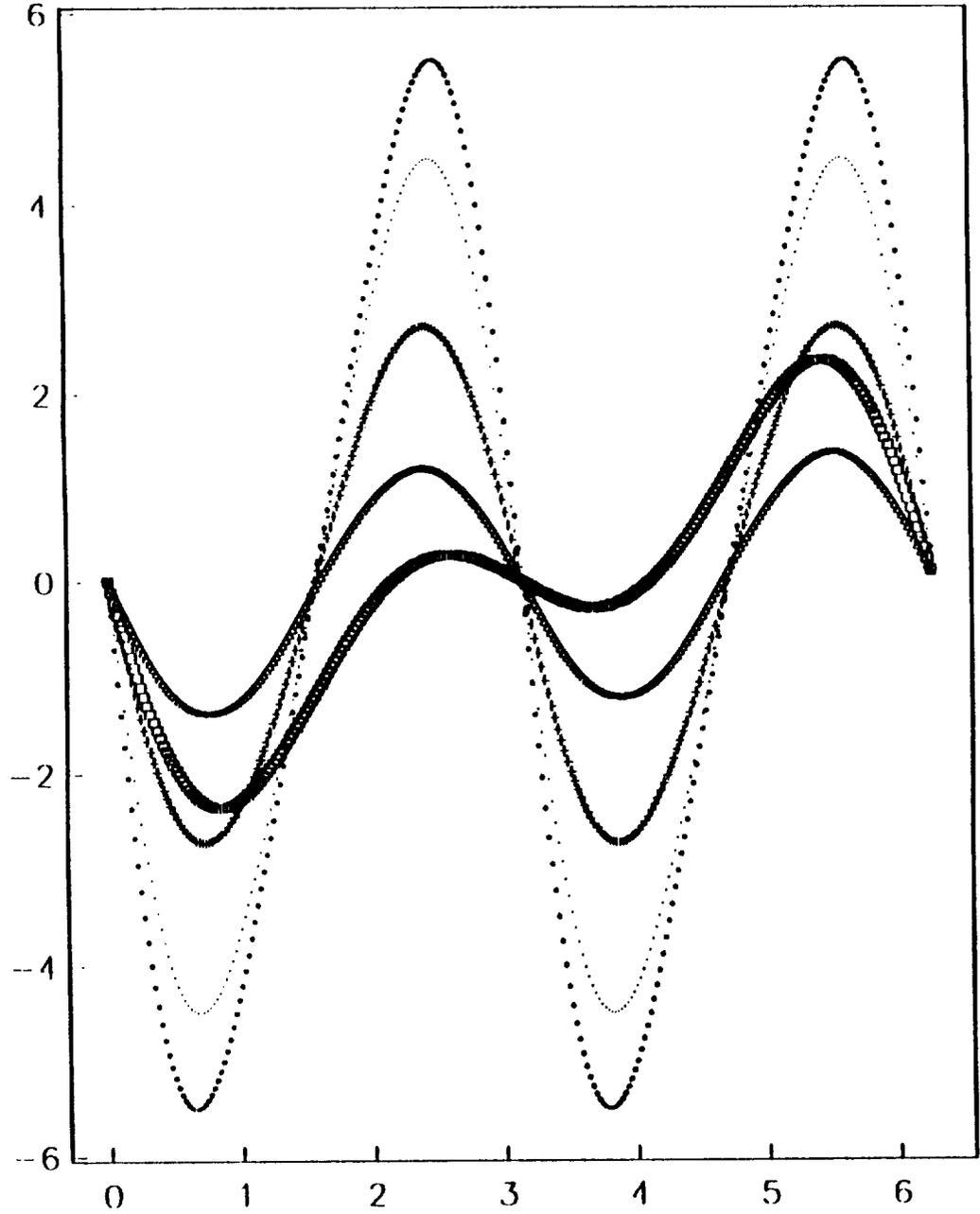
(a)

Circle=.2 Dot=.22 Plus=.24 Triangle=.248 Square=.28

Steady attracting profiles — ν= .08 .09 .12 .15 .2

(b)

Circle=.08 Dot=.09 Y=.12 Plus=.15 Triangle=.2
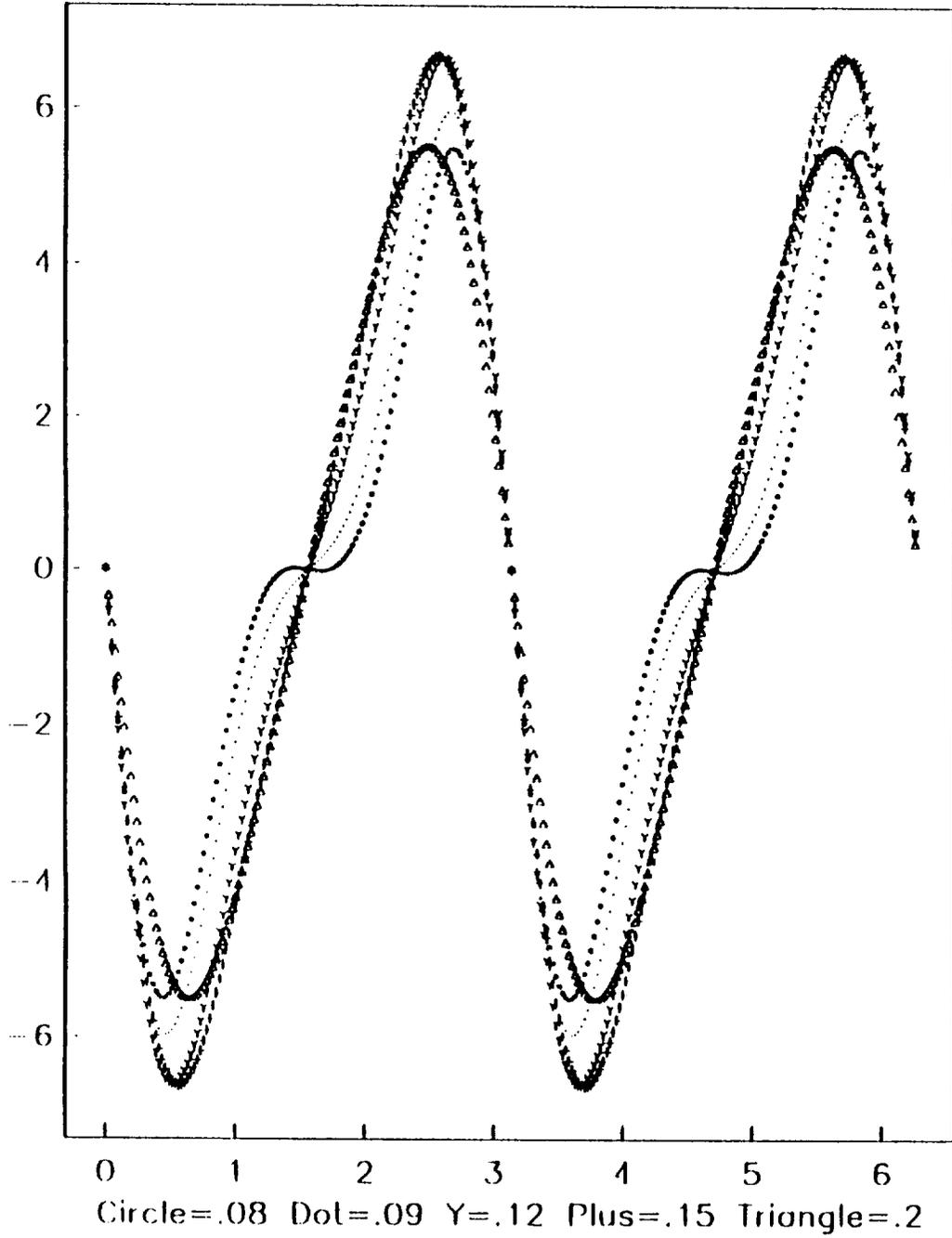
Figure (1.3)

Steady attracting profiles $\nu = .08\ .0755\ .074\ .072\ .07\ .067$

Square Triangle Plus Y Dot Circle
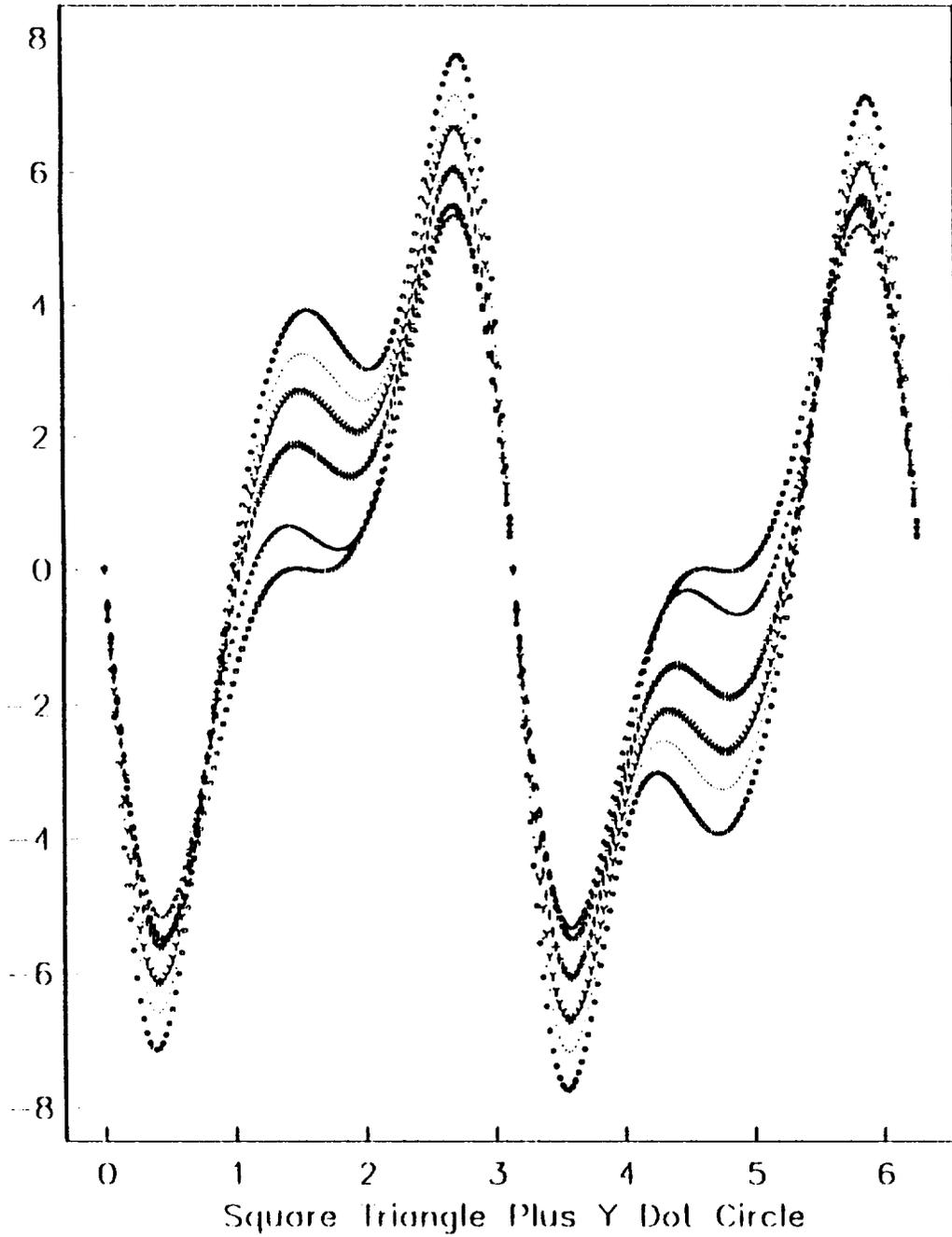
(a)

Steady attracting profiles $\nu=$ .06 .061 .063 .065 .06695

(b)

Square Triangle Plus Y Dot

(a)

Phase plane for Energy   v=.057

Period = 1.13   .34<t<5.3

Figure (2.1)

(b)

Energy against time   v=.057

Period = 1.13

(a)

Phase plane of Energy   v = .0559

Period = 2.367   —   51 < t < 64

Figure (2.2)

(b)

Energy against time   --   v = .0559

Period = 2.367

(a) Phase plane for Energy — v=.0555
Period = 2.48 — 40<t<58

Figure (2.3)

(b) Energy against time — v=.0555
Period = 2.48

(a)

(b)

(c)

Figure (3.1)

(a) Energy against time at v=.038. Time period = .684

(b) Phase plane for Energy at v=.038. Period = 0.684 - 5.3<t<20.1 in the trajectory plot - 21 time periods

(c) 1st Fourier coefficient against time for v=.038. Period=0.684

(d) 10th Fourier coefficient against time for v=.038. Period=0.684

Figure (4.1)

Phase plane for Energy at v=.03795

(a)

Energy against time at v=.03795

(b)

Period = 1.376

Figure (4.2)

Figure (4.3)

(a)

Phase plane of Energy - v=0.0376

Period = 2.87 - 5<t<18

(b)

6th Fourier coefficient against time for v=.0376

Period=2.872

Figure (4.4)

(c)

Phase plane for the 6th Fourier mode at v=.0376

Period=2.871 - 24.4<t<48.4 In the trajectory plot - Nine time periods

(a) Energy at v=.03736

Period T=3.019

(b) Phase plane for Energy at v=.03736

Period T=3.019 - 16<t<31

(c) Phase plane for Energy at v=.03735

Period = 1.51

Figure (4.5)

Figure (4.6)

Evolution of the profile within three time periods

Shift=6

v=.039 e=.0 Dt=.0296 Time Period= ..5915

Figure (4.7)

Evolution of the profile in a periodic attractor

V = .0375   shift = 5   Dt = .03

Energy against time for v=.0373

(a)
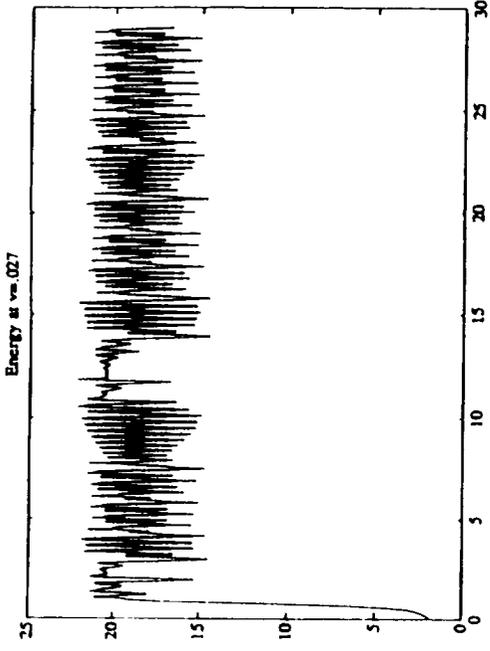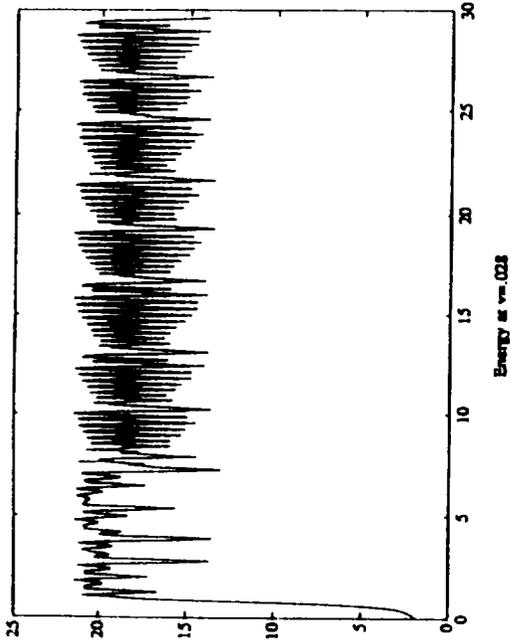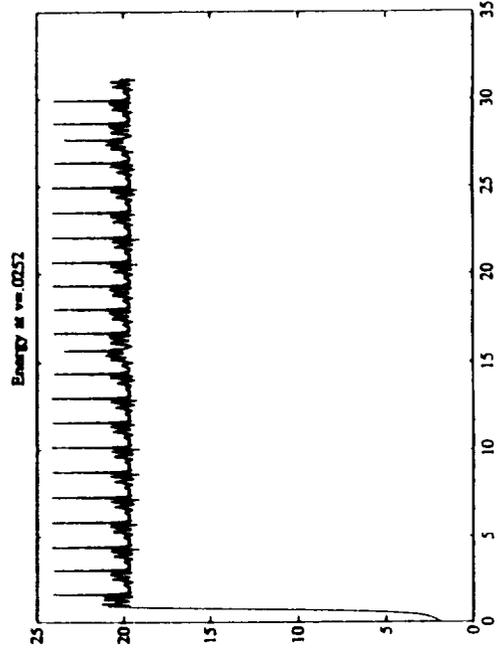
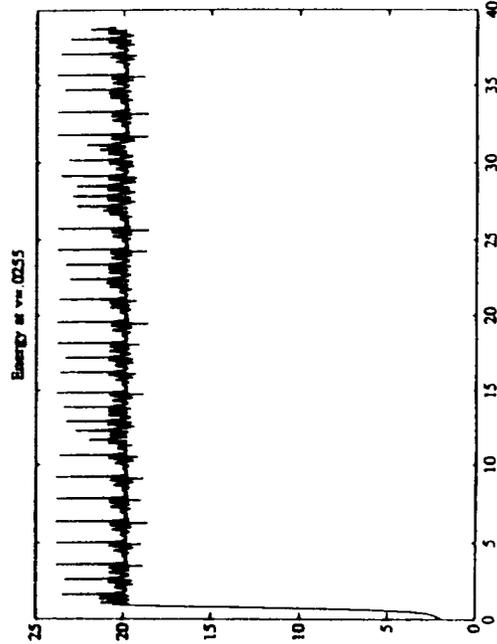Final profile for v=.0373

(b)

Figure (5.1)

(a)

(b)

(c)

(d)

Figure (6.1)

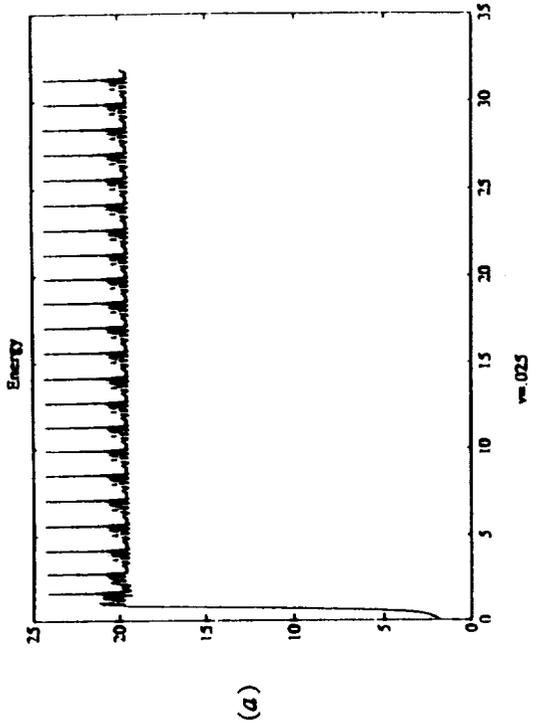(a)

(b)

(c)

(d)

Figure (6.2)

Figure (6.3)

(a)

Phase plane of Energy - v=0.02998

Period = 7.04 - 4.8<t<31.5 contains 4 periods

(b)

Phase plane of Energy - v=0.029978

Period = 7.04 - 9<t<31.5

(c)

Phase plane of Energy - v=0.0299756

Period = 7.04 - 3<t<31.5

Figure (6.4)

Figure (6.5)

Figure (7.1)

(a)

(b)

(c)

Energy

v = 025

Energy against time at v = 025

Time period = 1.426

Phase plane for Energy at v = 025

Time period = 1.426 - Time Trajectory [7,6,36,7]

Figure (8.1)

Figure (9.1)

NASA National Aeronautics and Space Administration	Report Documentation Page		
1. Report No. NASA CR-187461 ICASE Report No. 90-78	**2. Government Accession No.**	**3. Recipient's Catalog No.**	
4. Title and Subtitle THE ROUTE TO CHAOS FOR THE KURAMOTO-SIVASHINSKY EQUATION		**5. Report Date** October 1990	
		6. Performing Organization Code	
7. Author(s) Demetrious T. Papageorgiou Yiorgos S. Smyrlis		**8. Performing Organization Report No.** 90-78	
		10. Work Unit No. 505-90-21-01	
9. Performing Organization Name and Address Institute for Computer Applications in Science and Engineering Mail Stop 132C, NASA Langley Research Center Hampton, VA 23665-5225		**11. Contract or Grant No.** NAS1-18605	
12. Sponsoring Agency Name and Address National Aeronautics and Space Administration Langley Research Center Hampton, VA 23665-5225		**13. Type of Report and Period Covered** Contractor Report	
		14. Sponsoring Agency Code	

15. Supplementary Notes

Langley Technical Monitor: Richard W. Barnwell

Submitted to Theoretical and Computational Fluid Dynamics

Final Report

16. Abstract

We present the results of extensive numerical experiments of the spatially periodic initial value problem for the Kuramoto-Sivashinsky equation. Our concern is with the asymptotic nonlinear dynamics as the dissipation parameter decreases and spatio-temporal chaos sets in. To this end the initial condition is taken to be the same for all numerical experiments (a single sine wave is used) and the large time evolution of the system is followed numerically. Numerous computations were performed to establish the existence of windows, in parameter space, in which the solution has the following characteristics as the viscosity is decreased: A steady fully modal attractor to a steady bimodal attractor to another steady fully modal attractor to a steady trimodal attractor to a periodic (in time) attractor, to another steady fully modal attractor, to another time-periodic attractor, to a steady tetramodal attractor, to another time-periodic attractor having a full sequence of period-doublings (in the parameter space) to chaos. Numerous solutions are presented which provide conclusive evidence of the period-doubling cascades which precede chaos for this infinite-dimensional dynamical system. These results permit a computation of the lengths of subwindows which in turn provide an estimate for their successive ratios as the cascade develops. A calculation based on the numerical results is also presented to show that the period doubling sequences found here for the Kuramoto-Sivashinsky equation, are in complete agreement with Feigenbaum's universal constant of 4,669201609... . Some preliminary work shows several other windows following the first chaotic one including periodic, chaotic and a steady octamodal window; however the windows shrink significantly in size to enable concrete quantitative conclusions to be made.

17. Key Words (Suggested by Author(s)) Infinite-dimensional dynamical system, period-doubling, Feigenbaum number	**18. Distribution Statement** 34 - Fluid Mechanics and Heat Transfer Unclassified - Unlimited		
19. Security Classif. (of this report) Unclassified	**20. Security Classif. (of this page)** Unclassified	**21. No. of pages** 55	**22. Price** A04